Research Article Vol. 58, No. 15 / 20 May 2019 / Applied Optics 4143

applied optics

P_3 solution for the total steady-state and time-resolved reflectance and transmittance from a turbid slab

André Liemert,[1,*] Fabrizio Martelli,[2] Tiziano Binzoni,[3,4] and Alwin Kienle[1]

[1]Institut für Lasertechnologien in der Medizin und Meßtechnik, Helmholtzstr.12, D-89081 Ulm, Germany
[2]Dipartimento di Fisica e Astronomia dell'Università degli Studi di Firenze, Sesto Fiorentino, Firenze, Italy
[3]Département de Neurosciences Fondamentales, University of Geneva, Geneva, Switzerland
[4]Department of Radiology and Medical Informatics, University Hospital, Geneva, Switzerland
*Corresponding author: andre.liemert@ilm-ulm.de

Received 13 February 2019; revised 23 April 2019; accepted 24 April 2019; posted 25 April 2019 (Doc. ID 359956); published 20 May 2019

In this paper, we derive some explicit analytical solutions to the P_3 equations for the slab geometry that is illuminated by a collimated plane source. The resulting expressions for the total reflectance and transmittance are compared with the corresponding transport theory solution predicted by the Monte Carlo method. Further, for the special case of a non-absorbing anisotropically scattering slab, simple and accurate expressions in the P_1 approximation are obtained, yielding for optically thick slabs, the typical behavior of Ohm's law. In view of the time domain, we present an alternative method to the classical frequency-domain approach avoiding the use of complex numbers.

https://doi.org/10.1364/AO.58.004143

1. INTRODUCTION

The radiative transport equation (RTE) is a fundamental equation that is involved in many areas of science such as astrophysics, neutron transport, climate research, heat transfer, biomedical optics, and computer graphics [1–4]. It is considered to be the gold standard for prediction of the light propagation in random media, for example, biological tissue, because it provides in many cases a valid approximation of Maxwell's equations [5], avoiding the high demand for computer power needed for solving them. In the medical physics field, solutions to the RTE are often applied in the context of fluorescence spectroscopy, quantitative microscopy, bioluminescence imaging, or photodynamic therapy [6]. Until now, the diffusion equation has been the most often used approximation of the more complicated RTE. However, it is well known that the diffusion approximation fails in several situations of high practical importance. For example, solutions in diffusion approximation becomes inaccurate for small source-detector separations, short time values, small distances to boundaries, high spatial and temporal frequencies, highly absorbing media, as well as in inhomogeneous media (e.g., layered media). In view of numerical methods, the Monte Carlo method is the most often used approach for solving the RTE. For more details regarding this stochastic method, we refer to the article [7]. In recent years, different analytical approaches such as the method of rotated reference frames [8–10] or the singular eigenfunction method [11] have been developed for solving the RTE. Furthermore, the method of separation of variables has been used to find solutions of the two-dimensional RTE in the flatland geometry [12]. Also, several analytical solutions of the one-dimensional planar symmetric P_3 equations have been derived in recent years; see, for example, [13–16]. Apart from this, analytical solutions in the P_1 approximation have been presented in the publications [17–19]. In our previous work [20], we considered the solution of the three-dimensional P_3 equations in semi-infinite geometry. It has been shown via comparisons to the Monte Carlo method that the P_3 approximation leads to a significant improvement compared to classical diffusion theory [2].

In this paper, we derive analytical solutions of the P_3 equations for the slab geometry that is illuminated by a collimated plane source. In particular, we investigate the accuracy of the obtained expressions by comparing the total reflectance and transmittance with results predicted by the Monte Carlo method. Moreover, for the special case of a non-absorbing anisotropically scattering slab, simple and accurate expressions in the P_1 approximation are derived, showing the typical behavior of Ohm's law for slabs having a relatively large optical thickness [21]. Besides this, we present a method usable for reconstruction of time-resolved quantities such as the fluence, reflectance, or transmittance based on the corresponding solution in the steady-state domain. Compared with the classical frequency-domain approach, which takes into account a complex-valued absorption coefficient, the method presented here avoids the use of complex numbers.

2. SOLUTION OF THE P_3 EQUATIONS

The radiance $I(z,\mu)$ caused by an infinitely extended plane source obeys the RTE

$$\mu\partial_z I(z,\mu)+\sigma_t I(z,\mu)=\sigma_s\int_{-1}^{1} f(\mu,\eta)I(z,\eta)\mathrm{d}\eta+S(z,\mu), \quad (1)$$

where $(z,\mu)\in\mathbb{R}\times[-1,1]$, $\sigma_t=\sigma_a+\sigma_s$ is the attenuation coefficient with σ_a and σ_s as the absorption and scattering coefficient, respectively. The function $f(\mu,\eta):=\int_{-\pi}^{\pi} f\left(\mu\eta+\sqrt{1-\mu^2}\sqrt{1-\eta^2}\cos\varphi\right)\mathrm{d}\varphi$ is the scattering phase function integrated with respect to the azimuthal angle, and $S(z,\mu)$ denotes the source term. For the derivations outlined below, the scattering phase function is approximated by means of the delta-M method [22] of order $M=3$, yielding $f(\mu,\eta)\approx(1-f_4)\delta(\mu-\eta)+\tilde{f}(\mu,\eta)$ with

$$\tilde{f}(\mu,\eta)=\sum_{l=0}^{3}\frac{2l+1}{2}\frac{f_l-f_4}{1-f_4}P_l(\mu)P_l(\eta), \quad (2)$$

and P_l are the Legendre polynomials. The corresponding expansion coefficients are defined by $f_l=2\pi\int_{-1}^{1} f(\mu)P_l(\mu)\mathrm{d}\mu$ for $l=0,\ldots,4$. Furthermore, in order to obtain more accurate results, the radiance is separated into its ballistic and diffuse parts, such as $I:=I_0+I_d$ with $I_0(z,\mu)=\exp(-\tilde{\sigma}_t z)\Theta(z)\delta(1-\mu)$, where $\Theta(\cdot)$ denotes the Heaviside step function. The diffuse part satisfies the RTE

$$\begin{aligned}&\mu\partial_z I_d(z,\mu)+\tilde{\sigma}_t I_d(z,\mu)\\&\quad=\tilde{\sigma}_s\int_{-1}^{1}\tilde{f}(\mu,\eta)I_d(z,\eta)\mathrm{d}\eta+\tilde{\sigma}_s f(\mu,1)\exp(-\tilde{\sigma}_t z)\Theta(z), \quad (3)\end{aligned}$$

with the scaled coefficients $\tilde{\sigma}_t=\sigma_a+\tilde{\sigma}_s$ and $\tilde{\sigma}_s=(1-f_4)\sigma_s$. The associated exact radiative transfer boundary conditions for defining a slab of thickness L are given by

$$I_d(0,\mu)=R(\mu)I_d(0,-\mu),\qquad \mu>0, \quad (4)$$

$$I_d(L,\mu)=R(-\mu)I_d(L,-\mu),\qquad \mu<0, \quad (5)$$

with R being the Fresnel reflection coefficient defined as

$$R(\mu)=\frac{1}{2}\left(\frac{\mu-n\mu_0}{\mu+n\mu_0}\right)^2+\frac{1}{2}\left(\frac{\mu_0-n\mu}{\mu_0+n\mu}\right)^2,\qquad \mu>\mu_c, \quad (6)$$

where $n=n_i/n_e$, $\mu_0=\sqrt{1-n^2(1-\mu^2)}$, $\mu_c=\sqrt{n^2-1}/n$, and $R=1$ for $\mu<\mu_c$. To solve Eq. (3), the radiance is expanded in terms of the Legendre polynomials

$$I_d(z,\mu)=\sum_{l=0}^{3}\frac{2l+1}{2}\phi_l(z)P_l(\mu),\qquad \phi_l:=\langle I,P_l\rangle. \quad (7)$$

For more details regarding the P_N method, the readers may refer to the textbook [2]. In addition, the reader may refer in this context to the publications [13–16]. Inserting Eq. (7) into Eq. (3) leads to the following system of ordinary differential equations

$$\begin{aligned}&l\phi'_{l-1}+(2l+1)\sigma_l\phi_l+(l+1)\phi'_{l+1}\\&\quad=(2l+1)\sigma_s(f_l-f_4)\exp(-\tilde{\sigma}_t z)\Theta(z) \quad (8)\end{aligned}$$

for $l=0,\ldots,3$ with $\phi_{-1}=\phi_4=0$ and $\sigma_l=\sigma_a+(1-f_l)\sigma_s$. The associated boundary conditions belonging to this system are derived on the basis of the exact radiative transfer conditions from Eqs. (4) and (5) [23]. Inserting the series from Eq. (7) into these conditions, multiplying both sides with $P_{l'}$, and integrating over $|\mu|\le 1$ leads to

$$\begin{aligned}&\sum_{l=0}^{3}\frac{2l+1}{2}\phi_l(0)\int_0^1 P_l(\mu)P_{l'}(\mu)\mathrm{d}\mu\\&\quad=\sum_{l=0}^{3}\frac{2l+1}{2}\phi_l(0)\int_0^1 R(\mu)P_l(\mu)P_{l'}(\mu)\mathrm{d}\mu,\\&\sum_{l=0}^{3}\frac{2l+1}{2}\phi_l(L)\int_{-1}^0 P_l(\mu)P_{l'}(\mu)\mathrm{d}\mu\\&\quad=\sum_{l=0}^{3}\frac{2l+1}{2}\phi_l(L)\int_{-1}^0 R(-\mu)P_l(-\mu)P_{l'}(\mu)\mathrm{d}\mu.\end{aligned}$$

The resulting equations for $l'=1,3$ can be summarized as

$$\begin{aligned}&\left(\frac{1}{2}-R_{10}\right)\phi_0(0)+(1+3R_{11})\phi_1(0)+\left(\frac{5}{8}-5R_{12}\right)\phi_2(0)\\&\quad+7R_{13}\phi_3(0)=0,\\&\left(\frac{1}{8}+R_{30}\right)\phi_0(0)-3R_{13}\phi_1(0)-\left(\frac{5}{8}-5R_{23}\right)\phi_2(0)\\&\quad-(1+7R_{33})\phi_3(0)=0,\\&\left(\frac{1}{2}-R_{10}\right)\phi_0(L)-(1+3R_{11})\phi_1(L)+\left(\frac{5}{8}-5R_{12}\right)\phi_2(L)\\&\quad-7R_{13}\phi_3(L)=0,\\&\left(\frac{1}{8}+R_{30}\right)\phi_0(L)+3R_{13}\phi_1(L)-\left(\frac{5}{8}-5R_{23}\right)\phi_2(L)\\&\quad+(1+7R_{33})\phi_3(L)=0,\end{aligned}$$

where $R_{ll'}:=\int_0^1 R(x)P_l(x)P_{l'}(x)\mathrm{d}x$. Thus, the system of ordinary differential equations consists of four equations subject to four conditions. The general solution of the system from Eq. (8) is given by $\phi(z)=\phi^{(h)}(z)+\phi^{(p)}(z)$, where the homogenous part is found by setting $\phi^{(h)}(z)=v\exp(\lambda z)$. Inserting this ansatz into Eq. (8) results in

$$\begin{pmatrix}\sigma_0 & \lambda & 0 & 0\\ \lambda & 3\sigma_1 & 2\lambda & 0\\ 0 & 2\lambda & 5\sigma_2 & 3\lambda\\ 0 & 0 & 3\lambda & 7\sigma_3\end{pmatrix}v=0, \quad (9)$$

which can also be transformed into a standard eigenvalue problem according to

$$\begin{pmatrix}0 & -3\sigma_1 & 0 & 14\sigma_3/3\\ -\sigma_0 & 0 & 0 & 0\\ 0 & 0 & 0 & -7\sigma_3/3\\ 2\sigma_0/3 & 0 & -5\sigma_2/3 & 0\end{pmatrix}v=\lambda v. \quad (10)$$

The corresponding eigenvalues are given by

$$\lambda_1=\sqrt{\left(\alpha+\sqrt{\alpha^2-36\beta}\right)/18},$$

$$\lambda_2=\sqrt{\left(\alpha-\sqrt{\alpha^2-36\beta}\right)/18},$$

where $\alpha = 27\sigma_0\sigma_1 + 28\sigma_0\sigma_3 + 35\sigma_2\sigma_3$ and $\beta = 105\sigma_0\sigma_1\sigma_2\sigma_3$. The resulting homogenous solution can be written as

$$\phi_h(z) = C_1 \begin{pmatrix} x_0 \\ x_1 \\ x_2 \\ x_3 \end{pmatrix} e^{\lambda_1(z-L)} + C_2 \begin{pmatrix} x_0 \\ -x_1 \\ x_2 \\ -x_3 \end{pmatrix} e^{-\lambda_1 z} + C_3 \begin{pmatrix} y_0 \\ y_1 \\ y_2 \\ y_3 \end{pmatrix} e^{\lambda_2(z-L)} + C_4 \begin{pmatrix} y_0 \\ -y_1 \\ y_2 \\ -y_3 \end{pmatrix} e^{-\lambda_2 z}, \tag{11}$$

where C_i $(i = 0, \ldots, 3)$ are arbitrary constants. The components of the first eigenvector x have been obtained as

$$\begin{aligned} x_0 &= \frac{9}{2}\sigma_1\lambda_1^2 + \frac{14}{3}\sigma_3\lambda_1^2 - \frac{35}{2}\sigma_1\sigma_2\sigma_3, \\ x_1 &= \frac{35}{6}\sigma_2\sigma_3\lambda_1 - \frac{3}{2}\lambda_1^3, \\ x_2 &= -\frac{7}{3}\sigma_3\lambda_1^2 x, \\ x_3 &= \lambda_1^3, \end{aligned} \tag{12}$$

whereas those for y are obtained by interchanging λ_1 with λ_2. We note that the homogenous solution given above is valid under the restriction $\sigma_a \neq 0$. If $\sigma_a = 0$, it becomes

$$\begin{aligned} \phi_0^{(h)}(z) &= C_1 - 3\sigma_1 C_2 z - 2C_3 e^{\lambda(z-L)} - 2C_4 e^{-\lambda z}, \\ \phi_1^{(h)}(z) &= C_2, \\ \phi_2^{(h)}(z) &= C_3 e^{\lambda(z-L)} + C_4 e^{-\lambda z}, \\ \phi_3^{(h)}(z) &= \frac{3\lambda}{7\sigma_3} C_4 e^{-\lambda z} - \frac{3\lambda}{7\sigma_3} C_3 e^{\lambda(z-L)}, \end{aligned} \tag{13}$$

where $\lambda = \sqrt{35\sigma_2\sigma_3}/3$. The particular solution of Eq. (8) can be found via the method of variation of constants or by performing the ansatz $\phi^{(p)}(z) = v \exp(-\tilde{\sigma}_t z)$, where the unknown vector v follows as the solution of the following system of linear equations:

$$\begin{pmatrix} \sigma_0 & -\tilde{\sigma}_t & 0 & 0 \\ -\tilde{\sigma}_t & 3\sigma_1 & -2\tilde{\sigma}_t & 0 \\ 0 & -2\tilde{\sigma}_t & 5\sigma_2 & -3\tilde{\sigma}_t \\ 0 & 0 & -3\tilde{\sigma}_t & 7\sigma_3 \end{pmatrix} \begin{pmatrix} v_0 \\ v_1 \\ v_2 \\ v_3 \end{pmatrix} = \begin{pmatrix} \sigma_s(1-f_4)\exp(-\tilde{\sigma}_t z) \\ 3\sigma_s(f_1-f_4)\exp(-\tilde{\sigma}_t z) \\ 5\sigma_s(f_2-f_4)\exp(-\tilde{\sigma}_t z) \\ 7\sigma_s(f_3-f_4)\exp(-\tilde{\sigma}_t z) \end{pmatrix}. \tag{14}$$

As a result, the radiance in the P_3 approximation is found to be

$$I(z,\mu) = I_0(z,\mu) + I_d(z,\mu) = \exp(-\tilde{\sigma}_t z)\Theta(z)\delta(1-\mu) + \sum_{l=0}^{3} \frac{2l+1}{2}(\phi_l^{(h)}(z) + \phi_l^{(p)}(z))P_l(\mu). \tag{15}$$

Based on these results, the reflectance $R := -\int_{-1}^{1} \mu I(0,\mu)\mathrm{d}\mu$ and the transmittance $T := \int_{-1}^{1} \mu I(L,\mu)\mathrm{d}\mu$ can be calculated. In the absorbing case $(\sigma_a > 0)$, the reflected light is found to be

$$R = \frac{R_0 T_0 \exp(-2\tilde{\sigma}_t L)}{1 - R_0^2 \exp(-2\tilde{\sigma}_t L)} - C_1 x_1 \exp(-\lambda_1 L) + C_2 x_1 - C_3 y_1 \exp(-\lambda_2 L) + C_4 y_1 - v_1, \tag{16}$$

where $R_0 = (n_e - n_i)^2/(n_e + n_i)^2$ and $T_0 = 1 - R_0$ are the Fresnel reflection and transmission coefficients for normal incidence. The transmitted light becomes

$$T = \frac{T_0 \exp(-\tilde{\sigma}_t L)}{1 - R_0^2 \exp(-2\tilde{\sigma}_t L)} + C_1 x_1 - C_2 x_1 \exp(-\lambda_1 L) + C_3 y_1 - C_4 y_1 \exp(-\lambda_2 L) + v_1 \exp(-\tilde{\sigma}_t L). \tag{17}$$

If $\sigma_a = 0$, the reflectance and transmittance simplify to

$$\begin{aligned} R &= \frac{R_0 T_0 \exp(-2\tilde{\sigma}_t L)}{1 - R_0^2 \exp(-2\tilde{\sigma}_t L)} - C_2 - v_1, \\ T &= \frac{T_0 \exp(-\tilde{\sigma}_t L)}{1 - R_0^2 \exp(-2\tilde{\sigma}_t L)} + C_2 + v_1 \exp(-\tilde{\sigma}_t L). \end{aligned} \tag{18}$$

As shown below, the reflectance and transmittance in the P_3 approximation are in good agreement with the corresponding Monte Carlo results. However, for the non-absorbing case, there is the possibility to derive two simple closed-form solutions based on the P_1 equations. For this task, we have to consider the system

$$\phi_1' = \sigma_s(1 - f_2)\exp(-\tilde{\sigma}_s z)\Theta(z), \tag{19}$$

$$\phi_0' + 3\sigma_s'\phi_1 = 3\sigma_s(f_1 - f_2)\exp(-\tilde{\sigma}_s z)\Theta(z), \tag{20}$$

subject to the conditions $\phi_0(0) + 2A\phi_1(0) = 0$ and $\phi_0(L) - 2A\phi_1(L) = 0$, where $A = (1 + 3R_{11})/(1 - 2R_{10})$. Equation (19) can be integrated according to

$$\phi_1(z) = \sigma_s(1-f_2)\int \exp(-\tilde{\sigma}_t z)\Theta(z)\mathrm{d}z = C_1 + (1 - e^{-\tilde{\sigma}_t z})\Theta(z). \tag{21}$$

Inserting this result into Eq. (20) leads to

$$\begin{aligned} &\phi_0'(z) = 3\tilde{\sigma}_s \exp(-\tilde{\sigma}_s z)\Theta(z) - 3\sigma_s' C_1 - 3\sigma_s'\Theta(z) \\ &\Rightarrow \phi_0(z) = 3(1 - e^{-\tilde{\sigma}_t z})\Theta(z) - 3\sigma_s' z\Theta(z) - 3\sigma_s' C_1 z + C_2. \end{aligned} \tag{22}$$

The unknown constants C_1 and C_2 can now be determined from the boundary conditions yielding the diffuse reflectance $R_d = -\phi_1(0)$ and transmittance $T_d = \phi_1(L)$. In this context, we note on the particular values $\phi_0(0) = C_2$, $\phi_1(0) = C_1$, $\phi_0(L) = 3(1 - \exp(-\tilde{\sigma}_t L)) - 3\sigma_s' L - 3\sigma_s' C_1 L + C_2$, and $\phi_1(L) = C_1 + 1 - \exp(-\tilde{\sigma}_t L)$ and the required constants

$$\begin{aligned} C_1 &= \frac{(2A-3)\exp(-\tilde{\sigma}_t L) + 3(1 - \sigma_s' L) - 2A}{4A + 3\sigma_s' L}, \\ C_2 &= 2A\frac{(3-2A)\exp(-\tilde{\sigma}_t L) - 3(1 - \sigma_s' L) + 2A}{4A + 3\sigma_s' L}. \end{aligned}$$

Then the resulting complete solutions for the total reflectance and transmittance become

$$R = \frac{R_0 T_0 e^{-2\tilde{\mu}_s L}}{1 - R_0^2 e^{-2\tilde{\mu}_s L}} + \frac{(3D - z_e)(e^{-\tilde{\mu}_s L} - 1) + L}{L + 2z_e}, \tag{23}$$

$$T = \frac{T_0 e^{-\tilde{\mu}_s L}}{1 - R_0^2 e^{-2\tilde{\mu}_s L}} + \frac{(3D + z_e)(1 - e^{-\tilde{\mu}_s L}) - L e^{-\tilde{\mu}_s L}}{L + 2z_e}, \tag{24}$$

where $z_e = 2AD$ and $D = 1/(3\sigma_s')$. In the case of matched boundary conditions, when $n_r = 1$ and $z_e = 2D$, the above expressions reduce to

$$R = \frac{De^{-\tilde{\sigma}_s L} + L - D}{4D + L}, \qquad T = D\frac{5 - e^{-\tilde{\sigma}_s L}}{4D + L}. \tag{25}$$

For optically thick slabs, we obtain $T \sim 5D/L$, corresponding with Ohm's law for light that predicts an optical transmittance proportional to the inverse of the thickness of the slab.

3. RECONSTRUCTION OF TIME-DOMAIN RESULTS

In order to obtain the time-resolved reflectance and transmittance, we present in this section a method useable for reconstruction of these quantities based on the corresponding steady-state solution. In contrast to the classical frequency-domain approach, which takes into account a complex-valued absorption coefficient, the method presented below only requires the (real-valued) steady-state solution as function of the absorption. In practice, by taking the inverse Laplace transform of the steady-state solution over the variable σ_a, we directly obtain the time-dependent solution. In general, the inverse Laplace transform of a function $\hat{f}(s)$ $(s \in \mathbb{C})$ can be performed by means of the so-called Post–Widder formula

$$f(t) = \lim_{k\to\infty} \frac{(-1)^k}{k!}(k/t)^{k+1}\frac{d^k}{ds^k}\hat{f}(s)\bigg|_{s=k/t}.$$

A computable representation of this limit is given by the following truncated series [24]:

$$f(t) \approx \frac{\ln 2}{t}\sum_{k=1}^{N}\gamma_k \hat{f}(\eta_k), \tag{26}$$

with $\eta_k = k\ln(2)/t$ being the nodes and N being an even number. The corresponding weights are given by

$$\gamma_k = (-1)^{k+N/2}\sum_j \frac{j^{N/2}(2j)!}{(N/2-j)!j!(j-1)!(k-j)!(2j-k)!},$$

where $\lfloor (k+1)/2 \rfloor \le j \le \min(k, N/2)$. For the numerical experiments shown below, we use this formula for reconstruction of the time-resolved reflectance.

4. NUMERICAL EXPERIMENTS

In this section, numerical experiments are carried out in order to illustrate the accuracy of the derived analytical solutions. For this task, solutions were compared with results obtained from Monte Carlo simulations. The Monte Carlo method simulates the propagation of photons through the scattering medium using appropriate probability functions and the random number generator of the computer. In the limit of an infinitely large number of photons used in the simulations, the Monte Carlo method is an exact solution of the RTE. Our existing code was modified to be able to calculate the fluence, reflectance, and transmittance caused by an extended plane source. In all comparisons shown below the Henyey-Greenstein phase function is considered. In Fig. 1, we simulated the total reflectance and transmittance due to an incident beam for two different relative refractive indices, namely, $n = 1.0$ and $n = 1.4$.

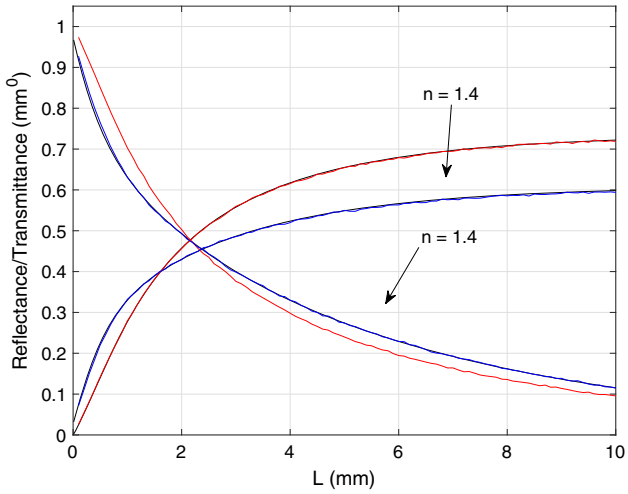

Fig. 1. Total reflectance and transmittance due to an incident beam for two different relative refractive indices. The optical properties of the slab are set to $\sigma_a = 0.01$ mm^{-1}, $\sigma_s' = 0.9$ mm^{-1}, and $g = 0.8$.

The solution in the P_3 approximation is denoted by the smooth lines, whereas the noisy curves represent the solution predicted by the Monte Carlo method.

Due to the small differences between the P_3 approximation and the Monte Carlo results, we have computed the relative errors versus the slab thickness and included them in Fig. 2. It can be seen that the smaller the thickness of the slab, the larger relative errors are. We additionally computed the relative errors between the Monte Carlo method and the solution in the P_{13} approximation corresponding with the green line. The agreement with the Monte Carlo data is within the stochastic errors of this method.

For the next comparison, we have considered the total reflectance for the case of a higher absorption coefficient. Figure 3 shows a comparison between the results obtained with the Monte Carlo simulation (noisy curve), the P_3 approximation (solid line), and additionally the P_1 approximation (dashed line). It should be noted that the solution in the P_1 approximation

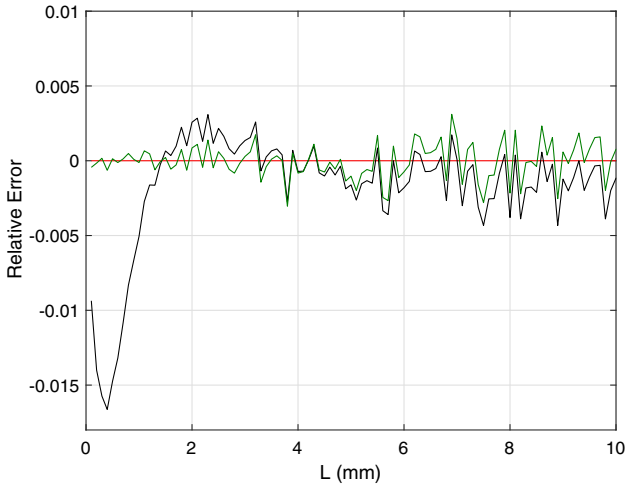

Fig. 2. Relative error versus thickness of the slab for the transmittance in the case of $n = 1.4$.

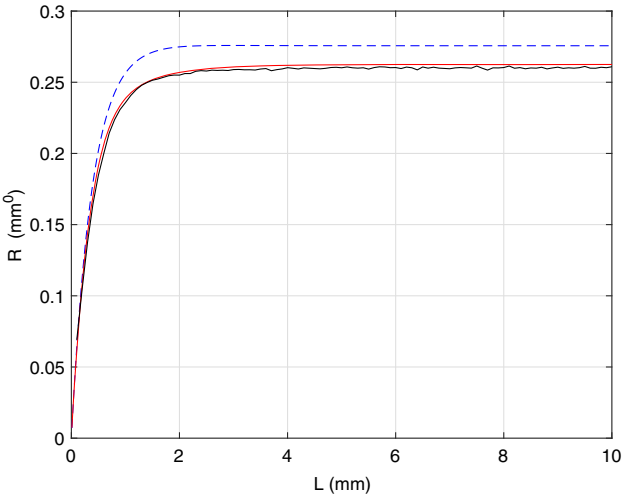

Fig. 3. Total reflectance due to an incident beam. The optical properties of the slab are set to $\sigma_a = 0.1$ mm^{-1}, $\sigma_s' = 1$ mm^{-1}, $g = 0.8$, and $n = 1.4$.

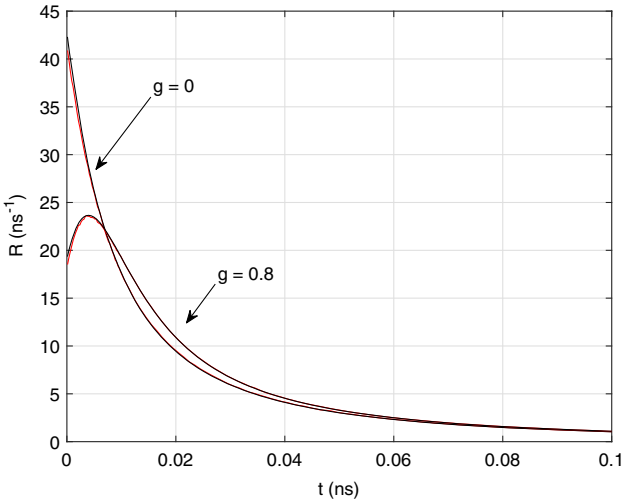

Fig. 5. Time-resolved reflectance from a scattering slab of thickness $L = 14$ mm. The optical properties are assumed to be $\sigma_a = 0.01$ mm^{-1}, $\sigma_s' = 0.9$ mm^{-1}, and $n = 1.0$.

corresponds, in principle, with the solution of the diffusion equation subject to the partial current boundary conditions (including a modified source term). The optical properties of the scattering slab are assumed to be $\sigma_a = 0.1$ mm^{-1}, $\sigma_s' = 1$ mm^{-1}, $g = 0.8$, and $n = 1.4$. It can be seen that the solution in the P_1 approximation shows significant differences to the exact transport theory reflectance.

In Fig. 4, we compared the simple formulae for the reflectance and transmittance given in Eq. (25) for a non-absorbing slab with Monte Carlo simulations. We have considered both isotropic and anisotropic scattering. In the latter case, the Henyey–Greenstein phase function has been considered. As can be seen, the derived formulae lead in all cases to quite good agreement. We note that for mismatched boundary conditions the agreement is significantly worse.

We proceed further with the reconstruction of the time-resolved reflectance from a scattering slab based on the algorithm presented in Eq. (26). Figure 5 shows the reflectance in the time domain for two different anisotropic factors of the Henyey–Greenstein phase function subject to matched boundary conditions. A good agreement between the P_3 approximation and the results predicted by the Monte Carlo method is observed.

In Fig. 6, we repeated the last numerical experiment for the case of mismatched boundary conditions. Similar to in the case of matched conditions, the solution in the P_3 approximation is in good agreement with the exact transport theory solution obtained via the Monte Carlo method.

In Fig. 7, we compared the fluence $\Phi := \int_{-1}^{1} I(z,\mu)\mathrm{d}\mu$ within a scattering slab with Monte Carlo simulations (filled dots). In order to demonstrate the accuracy of the derived solutions in the P_3 approximation, we additionally have included the solution in the P_1 approximation.

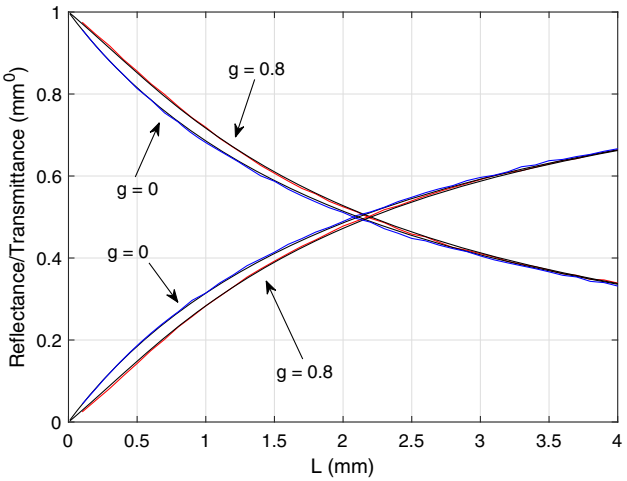

Fig. 4. Total reflectance and transmittance due to an incident beam for two different anisotropic factors. The optical properties of the slab are set to $\sigma_a = 0$ mm^{-1}, $\sigma_s' = 0.9$ mm^{-1}, and $n = 1.0$.

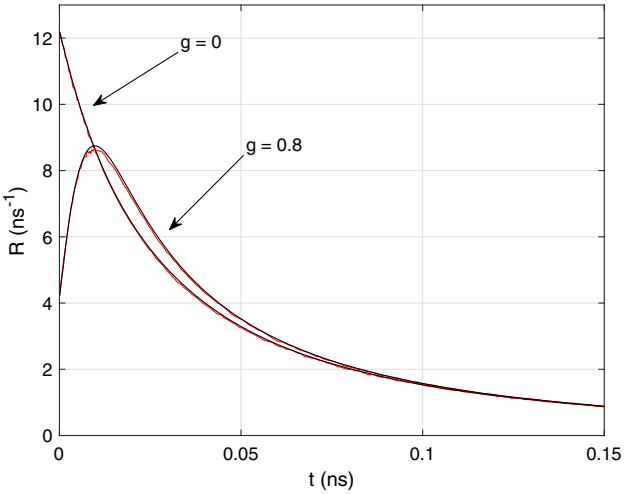

Fig. 6. Time-resolved reflectance from a scattering slab of thickness $L = 14$ mm. The optical properties are assumed to be $\sigma_a = 0.01$ mm^{-1}, $\sigma_s' = 0.9$ mm^{-1}, and $n = 1.4$.

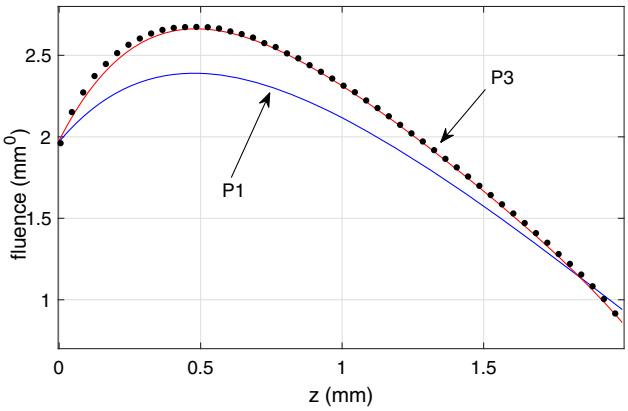

Fig. 7. Fluence within a scattering slab of thickness $L = 2$ mm. The optical properties are assumed to be $\sigma_a = 0.01$ mm^{-1}, $\sigma_s' = 1$ mm^{-1}, $g = 0.8$, and $n = 1.0$.

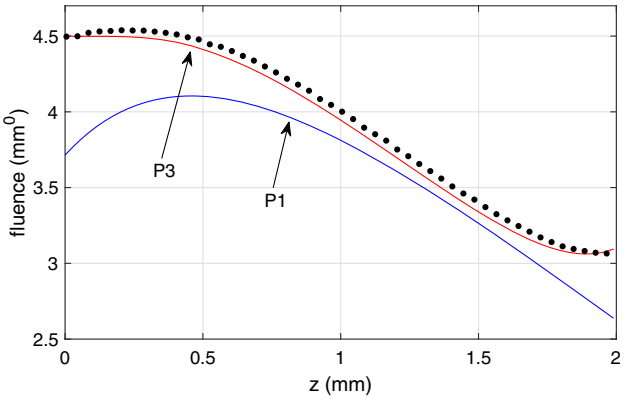

Fig. 8. Fluence within a scattering slab of thickness $L = 2$ mm. The optical properties are assumed to be $\sigma_a = 0.01$ mm^{-1}, $\sigma_s' = 1$ mm^{-1}, $g = 0.8$, and $n = 1.4$.

In Fig. 8, we repeated the last numerical experiment for the case of mismatched boundary conditions. Again, there is a significant improvement of the P_3 approximation over the fluence in the P_1 approximation.

5. CONCLUDING REMARKS

In this paper, we have derived some explicit analytical solutions to the P_3 equations for slab geometry, which is illuminated by a collimated plane source. The resulting expressions for the total reflectance and transmittance have been compared with Monte Carlo simulations. It has been shown that the solutions to the P_3 equations are in quite good agreement with the results predicted by the Monte Carlo method. For the special case of a non-absorbing anisotropically scattering slab, simple and accurate expressions in the P_1 approximation have been obtained, showing the typical behavior of Ohm's law for slabs with relatively large optical thickness. Concerning the time domain, we have proposed a method usable for reconstruction of time-resolved quantities based on the corresponding solution in the steady-state domain. Compared with the classical frequency domain approach, this method avoids the use of complex numbers.

Funding. Deutsche Forschungsgemeinschaft (DFG).

REFERENCES

1. A. Ishimaru, *Wave Propagation and Scattering in Random Media* (Academic, 1978).
2. K. M. Case and P. F. Zweifel, *Linear Transport Theory* (Addison-Wesley, 1967).
3. F. Martelli, S. Del Bianco, A. Ismaelli, and G. Zaccanti, *Light Propagation Through Biological Tissue and Other Diffusive Media: Theory, Solutions, and Software* (SPIE, 2010).
4. E. d'Eon and G. Irving, "A quantized-diffusion model for rendering translucent materials," ACM Trans. Graph. **30**, 56:1–56:12 (2011).
5. M. I. Mishchenko, L. D. Travis, and A. A. Lacis, *Multiple Scattering of Light by Particles* (Cambridge University, 2006).
6. D. A. Boas, C. Pitris, and P. F. Ramanujam, *Handbook of Biomedical Optics* (CRC Press, 2012).
7. L. Wang, S. L. Jacques, and L. Zheng, "MCML-Monte Carlo modeling of light transport in multi-layered tissues," Comput. Methods Programs Biomed. **47**, 131–146 (1995).
8. V. A. Markel, "Modified spherical harmonics method for solving the radiative transport equation," Waves in Random & Complex Media **14**, L13–L19 (2004).
9. A. Liemert and A. Kienle, "Green's function of the time-dependent radiative transport equation in terms of rotated spherical harmonics," Phys. Rev. E **86**, 036603 (2012).
10. M. Machida, G. Y. Panasyuk, J. C. Schotland, and V. A. Markel, "The Green's function for the radiative transport equation in the slab geometry," J. Phys. A **43**, 065402 (2010).
11. M. Machida, "Singular eigenfunctions for the three-dimensional radiative transport equation," J. Opt. Soc. Am. A **31**, 67–74 (2014).
12. M. Machida, "The radiative transport equation in flatland with separation of variables," J. Math. Phys. **57**, 073301 (2016).
13. Y. Bayazitoilu and J. Higenyi, "Higher-order differential equations of radiative transfer: P3 approximation," AIAA J. **17**, 424–431 (1979).
14. W. M. Star, "Comparing the P3-approximation with diffusion theory and with Monte Carlo calculations of light propagation in a slab geometry," Proc. SPIE **10305**, 103050C (1989).
15. D. Dickey, O. Barajas, K. Brown, J. Tulip, and R. B. Moore, "Radiance modelling using the P3 approximation," Phys. Med. Biol. **43**, 3559–3570 (1998).
16. E. L. Hull and T. H. Foster, "Steady-state reflectance spectroscopy in the P3 approximation," J. Opt. Soc. Am. A **18**, 584–599 (2001).
17. T. Spott and L. O. Svaasand, "Collimated light sources in the diffusion approximation," Appl. Opt. **39**, 6453–6465 (2000).
18. S. A. Carp, S. A. Prahl, and V. Venugopalan, "Radiative transport in the delta-P1 approximation: accuracy of fluence rate and optical penetration depth predictions in turbid semi-infinite media," J. Biomed. Opt. **9**, 632–648 (2004).
19. I. Seo, C. K. Hayakawa, and V. Venugopalan, "Radiative transport in the delta-approximation for semi-infinite turbid media," Med. Phys. **35**, 681–693 (2008).
20. A. Liemert and A. Kienle, "Explicit solutions of the radiative transport equation in the P_3 approximation," Medical physics **41**, 111916 (2014).
21. D. J. Durian, "Influence of boundary reflection and refraction on diffusive photon transport," Phys. Rev. E **50**, 857–866 (1994).
22. W. J. Wiscombe, "The delta-M method: rapid yet accurate radiative flux calculations for strongly asymmetric phase functions," J. Atmos. Sci. **34**, 1408–1422 (1977).
23. M. F. Modest, *Radiative Heat Transfer* (Academic, 2003).
24. K. L. Kuhlman, "Review of inverse Laplace transform algorithms for Laplace-space numerical approaches," Numer. Algorithm **63**, 339–355 (2013).